Hindawi
Advances in High Energy Physics
Volume 2023, Article ID 6057292, 17 pages
https://doi.org/10.1155/2023/6057292

Research Article

The Geometric Correlations of Leptonic Mixing Parameters

Ding-Hui Xu and Shu-Jun Rong

College of Science, Guilin University of Technology, Guilin, Guangxi 541004, China

Correspondence should be addressed to Shu-Jun Rong; rongshj@glut.edu.cn

Received 28 September 2022; Revised 3 February 2023; Accepted 24 February 2023; Published 21 March 2023

Academic Editor: Theocharis Kosmas

Leptonic mixing patterns are usually extracted on the basis of groups or algebraic structures. In this paper, we introduce an alternative geometric method to study the correlations between the leptonic mixing parameters. At the 3σ level of the recent global fit data of neutrino oscillations, the distribution of the scattered points of the angles between the vectors, which are constructed by the element of the leptonic mixing matrix, is analysed. We find that the scattered points are concentrated on several special regions. Using the data in these regions, correlations of the leptonic mixing angles and the Dirac CP violating phase are obtained. The implications of the correlations are shown through the predicted flavor ratio of high-energy astrophysical neutrinos (HANs) at Earth.

1. Introduction

The discovery of neutrino flavor oscillation is a tremendous achievement in particle physics during the last two decades [1–3], which manifests that neutrinos have masses, and the leptonic mixing matrix is nontrivial. However, the origin of the flavor mixing is elusive for theorists. Before the determination of the reactor mixing angle θ_{13}, the following are various candidates of the mixing patterns: bimaximal mixing (BM) [4], tri-bi-maximal mixing (TBM) [5, 6], golden ratio mixing (GRM) [7–9], hexagonal mixing (HM) [10], etc.[11, 12] (for reviews, see [13, 14]). These patterns, especially the TBM, derived from flavor groups such as A_4 [15, 16] and S_4 [16, 17], are compatible with previous published data of atmospheric neutrino and solar neutrino. The discovery of a relatively large reactor mixing angle θ_{13} [3, 18–21] and the remarkable progress of measurements of neutrino oscillation parameters, however, strictly constrain or exclude the above patterns. Hence, diverse methods to generate a nonzero reactor mixing angle θ_{13} have been proposed. A popular approach is adding a model-independent perturbation to the leading TBM matrix [22]. Another method introduces a generalized CP transform on the basis of a discrete flavor symmetry, i.e., a finite flavor group G_f and a CP symmetry are combined [23–27]. Furthermore, a novel mathematical structure called group algebra was introduced [28, 29]. In this scenario, a specific leptonic mixing pattern could correspond to a set of equivalent elements of a group algebra.

In this paper, we introduce an alternative geometric method to extract the correlations between the leptonic mixing parameters. This method is developed from the well-known $\mu-\tau$ reflection symmetry [30–39] which denotes that two row vectors $\vec{\mu}=(|U_{\mu1}|^2,|U_{\mu2}|^2,|U_{\mu3}|^2)$ and $\vec{\tau}=(|U_{\tau1}|^2,|U_{\tau2}|^2,|U_{\tau3}|^2)$ are identical. Here, $U_{\alpha i}(\alpha=\mu,\tau,\text{and } i=1,2,3)$ is the element of the Pontecorvo-Maki-Nakagawa-Sakata (PMNS) mixing matrix [40–42]

$$U=\begin{pmatrix} c_{12}c_{13} & s_{12}c_{13} & s_{13}e^{-i\delta} \\ -s_{12}c_{23}-c_{12}s_{13}s_{23}e^{i\delta} & c_{12}c_{23}-s_{12}s_{13}s_{23}e^{i\delta} & c_{13}s_{23} \\ s_{12}s_{23}-c_{12}s_{13}c_{23}e^{i\delta} & -c_{12}s_{23}-s_{12}s_{13}c_{23}e^{i\delta} & c_{13}c_{23} \end{pmatrix}, \tag{1}$$

where $s_{ij}\equiv\sin\theta_{ij}$ (for $ij=12,\ 13,\ 23$), $c_{ij}\equiv\cos\theta_{ij}$, and δ is the Dirac CP phase. Throughout this article, we do not consider the Majorana phases because they are irrelevant to neutrino oscillations. As is known, for the realistic mixing

matrix, the $\mu-\tau$ reflection symmetry predicts that $\theta_{23}=\pi/4$ and $\delta=\pm\pi/2$. According to the recent global analysis NuFIT 5.0 [43], the maximal CP phase is favored by the 1σ allowed region in the case of inverted mass ordering (IO) while disfavored by the 1σ allowed region in the normal ordering (NO) case. Therefore, the $\mu-\tau$ reflection symmetry may need modifications in the near future when a precise measurement of δ would be available.

Geometrically speaking, the $\mu-\tau$ reflection symmetry means that the angle between the 3-dimensional real vectors $\vec{\mu}$ and $\vec{\tau}$ is zero. A perturbed $\mu-\tau$ symmetry corresponds to a small but nonzero included angle. Thus, the leptonic mixing pattern and the breaking of $\mu-\tau$ reflection symmetry can be represented by the geometric quantities, namely, the angles between the row vectors $\vec{\mu}$, $\vec{\tau}$, and $\vec{e}=(|U_{e1}|^2,|U_{e2}|^2,|U_{e3}|^2)$. In order to extract promising mixing patterns, we scan the included angles between the row vectors at the 3σ level of the global fit data [43]. We find that the scattered points of the angles are concentrated on several special areas which are stable under the random takings of the mixing parameters at the 3σ level. Furthermore, it is not surprising that the approximated $\mu-\tau$ reflection symmetry corresponds to one of the special regions in the case of IO. Therefore, it is plausible that the promising correlations of the mixing parameters are indicated in these dense regions. On the basis of this assumption, the leptonic mixing patterns are read out from the dense zones and their implications are examined by a specific application, namely, the predicted flavor ratio of high-energy astrophysical neutrinos (HANs) at Earth.

The paper is organized as follows. In Section 2, we show the definition of included angles between the row vectors $\vec{e}$, $\vec{\mu}$, and $\vec{\tau}$ and extract correlations of the angles at the 3σ level of the global fit data [43]. On the basis of the correlations of the angles, the correlations of the leptonic mixing parameters are obtained. In Section 3, we apply these leptonic mixing parameters constrained by the geometric correlations to predict the flavor ratio of HANs at Earth. Finally, we summarize our main results.

2. Geometric Correlations at the 3σ Level of the Global Fit Data

In this section, we first give the definition of the angles between the row vectors, the selection rule of typical data points in the dense zones of the scattered plots, and then present correlations between the angles, on the basis of which we derive the correlations between the leptonic mixing parameters.

2.1. Definition of Geometric Correlations. The included angles between the row vectors are defined as follows:

$$\cos\left(\vec{\mu},\vec{\tau}\right)\equiv\frac{\vec{\mu}\cdot\vec{\tau}}{\left|\vec{\mu}\right|\cdot\left|\vec{\tau}\right|}=\frac{|U_{\mu1}|^2|U_{\tau1}|^2+|U_{\mu2}|^2|U_{\tau2}|^2+|U_{\mu3}|^2|U_{\tau3}|^2}{\sqrt{|U_{\mu1}|^4+|U_{\mu2}|^4+|U_{\mu3}|^4}\cdot\sqrt{|U_{\tau1}|^4+|U_{\tau2}|^4+|U_{\tau3}|^4}},$$

$$\cos\left(\vec{e},\vec{\mu}\right)\equiv\frac{\vec{e}\cdot\vec{\mu}}{\left|\vec{e}\right|\cdot\left|\vec{\mu}\right|}=\frac{|U_{e1}|^2|U_{\mu1}|^2+|U_{e2}|^2|U_{\mu2}|^2+|U_{e3}|^2|U_{\mu3}|^2}{\sqrt{|U_{e1}|^4+|U_{e2}|^4+|U_{e3}|^4}\cdot\sqrt{|U_{\mu1}|^4+|U_{\mu2}|^4+|U_{\mu3}|^4}},$$

$$\cos\left(\vec{e},\vec{\tau}\right)\equiv\frac{\vec{e}\cdot\vec{\tau}}{\left|\vec{e}\right|\cdot\left|\vec{\tau}\right|}=\frac{|U_{e1}|^2|U_{\tau1}|^2+|U_{e2}|^2|U_{\tau2}|^2+|U_{e3}|^2|U_{\tau3}|^2}{\sqrt{|U_{e1}|^4+|U_{e2}|^4+|U_{e3}|^4}\cdot\sqrt{|U_{\tau1}|^4+|U_{\tau2}|^4+|U_{\tau3}|^4}}.\quad(2)$$

Table 1: The 3σ allowed ranges of the leptonic mixing parameters in the global analysis NuFIT 5.0 [43].

Parameters	Normal ordering (NO)	Inverted ordering (IO)
$\sin^2\theta_{12}$	0.269→0.343	0.269→0.343
$\sin^2\theta_{13}$	0.02034→0.02430	0.02053→0.02436
$\sin^2\theta_{23}$	0.407→0.618	0.411→0.621
$\delta/^\circ$	107→403	192→360

Using the latest global fit data of the leptonic mixing parameters listed in Table 1, the 3σ allowed ranges of the included angle between the row vectors are shown in Figure 1.

We can see that the data points in these plots are of a nonuniform distribution. There are several special regions on which the points are concentrated. This observation is more obvious in the front view and top view of the plots shown in Figure 2.

From the 2-dimensional scattered plots, we obtain the observations as follows:

(a) NO case: the data points of $(\cos(\vec{\mu},\vec{\tau}),\cos(\vec{e},\vec{\mu}))$ are concentrated on two regions around the points (0.96, 0.40) and (0.96, 0.59), respectively. The data points of $(\cos(\vec{\mu},\vec{\tau}),\cos(\vec{e},\vec{\tau}))$ are also converged on two regions around the points (0.96, 0.39) and (0.96, 0.58), respectively

(b) IO case: the data points of $(\cos(\vec{\mu},\vec{\tau}),\cos(\vec{e},\vec{\mu}))$ are concentrated on three regions around the points (0.96, 0.41), (0.96, 0.60), and (1.00, 0.49), respectively. The data points of $(\cos(\vec{\mu},\vec{\tau}),\cos(\vec{e},\vec{\tau}))$ are converged on three regions around the points (0.96, 0.39), (0.96, 0.60), and (1.00, 0.48), respectively. As is known, $\cos(\vec{\mu},\vec{\tau})\sim1$ corresponds to the approximated $\mu-\tau$ reflection symmetry

Furthermore, we note that these dense zones of the scattered plots are stable under the random takings of the global fit data at 3σ level. Therefore, we consider that the global fit data indicate correlations between the included angles of the row vectors. Correspondingly, besides the leptonic mixing pattern

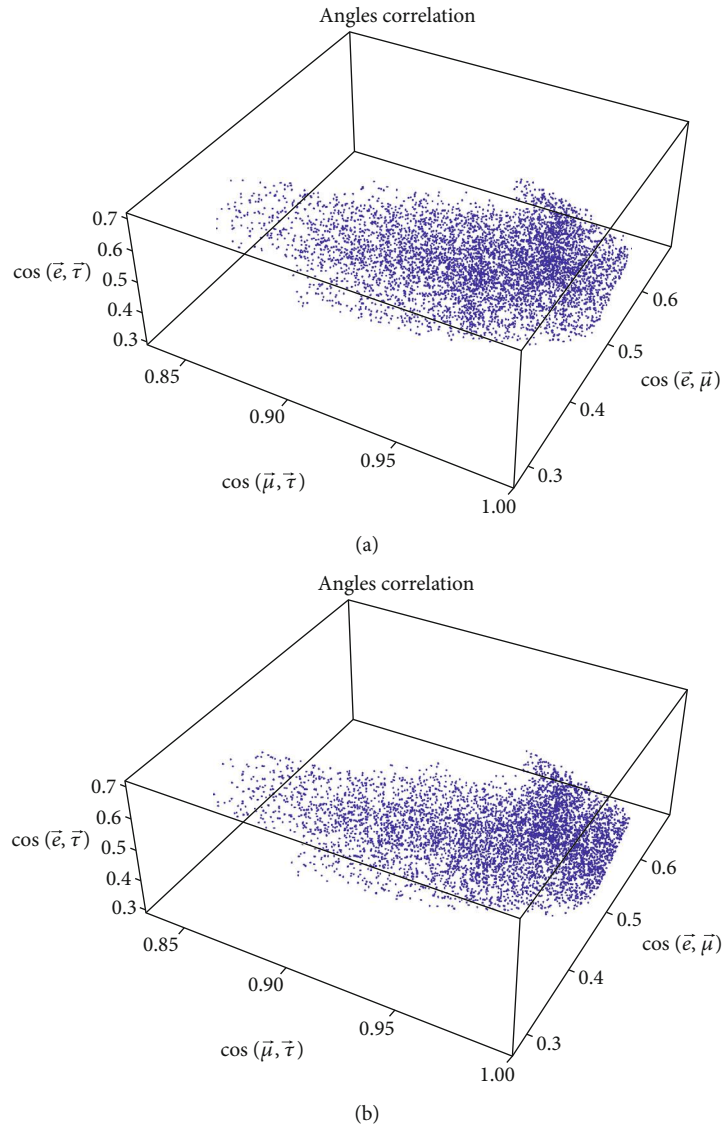

Figure 1: Three-dimensional scattered plots of the included angles based on the recent global fit data listed in Table 1. (a) NO case. (b) IO case.

from the approximated $\mu - \tau$ reflection symmetry, other promising patterns or correlations of the mixing parameters can be read out from the dense regions in the scattered plots.

2.2. Selection Rule of Typical Data Points in the Dense Regions of the Scattered Plots. In order to effectively filter out some representative data points in the dense zones of Figure 2, we divide the data samples of the angles between the row vectors into small enough intervals. The advantage of this method is that the difference between the impacts of two arbitrary data points in the same interval on the correlations of the lepton mixing parameters can be ignored. In other words, we can use the midpoint to represent the whole interval. The selection rule is explained in more detail as follows.

We divide the data samples of $\cos(\vec{\mu}, \vec{\tau})$ originated from Figure 2 into a series of small intervals such as [0.825, 0.835], ⋯, [0.955, 0.965],⋯, [0.995, 1.00], which are shown in Figure 3.

From Figure 3, we can observe that the number of data points with $\cos(\vec{\mu}, \vec{\tau}) \in [0.955, 0.965]$ is maximal both in the NO case and IO case. In consequence, we focus on the interval of $\cos(\vec{\mu}, \vec{\tau})$, [0.955, 0.965]. Based on the similar approach, the number of data points of $\cos(\vec{e}, \vec{\mu})$ and $\cos(\vec{e}, \vec{\tau})$ is presented in Figure 4, with the constraint of $|\cos(\vec{\mu}, \vec{\tau}) - 0.96| < 0.005$.

From Figure 4, we can see that the large numbers of scattered points in several intervals are approximate in the IO case, e.g., the $\cos(\vec{e}, \vec{\mu})$ intervals [0.575, 0.585] and [0.595, 0.605] and the $\cos(\vec{e}, \vec{\tau})$ intervals [0.375, 0.385], [0.385, 0.395], and [0.405, 0.415]. However, the numerical results show that these intervals with a similar number of scattered points in the same dense region bring no obvious differences on the correlations of the lepton mixing parameters. Therefore, for the sake of illustration, we select the intervals of $\cos(\vec{e}, \vec{\mu})$ and $\cos(\vec{e}, \vec{\tau})$ with

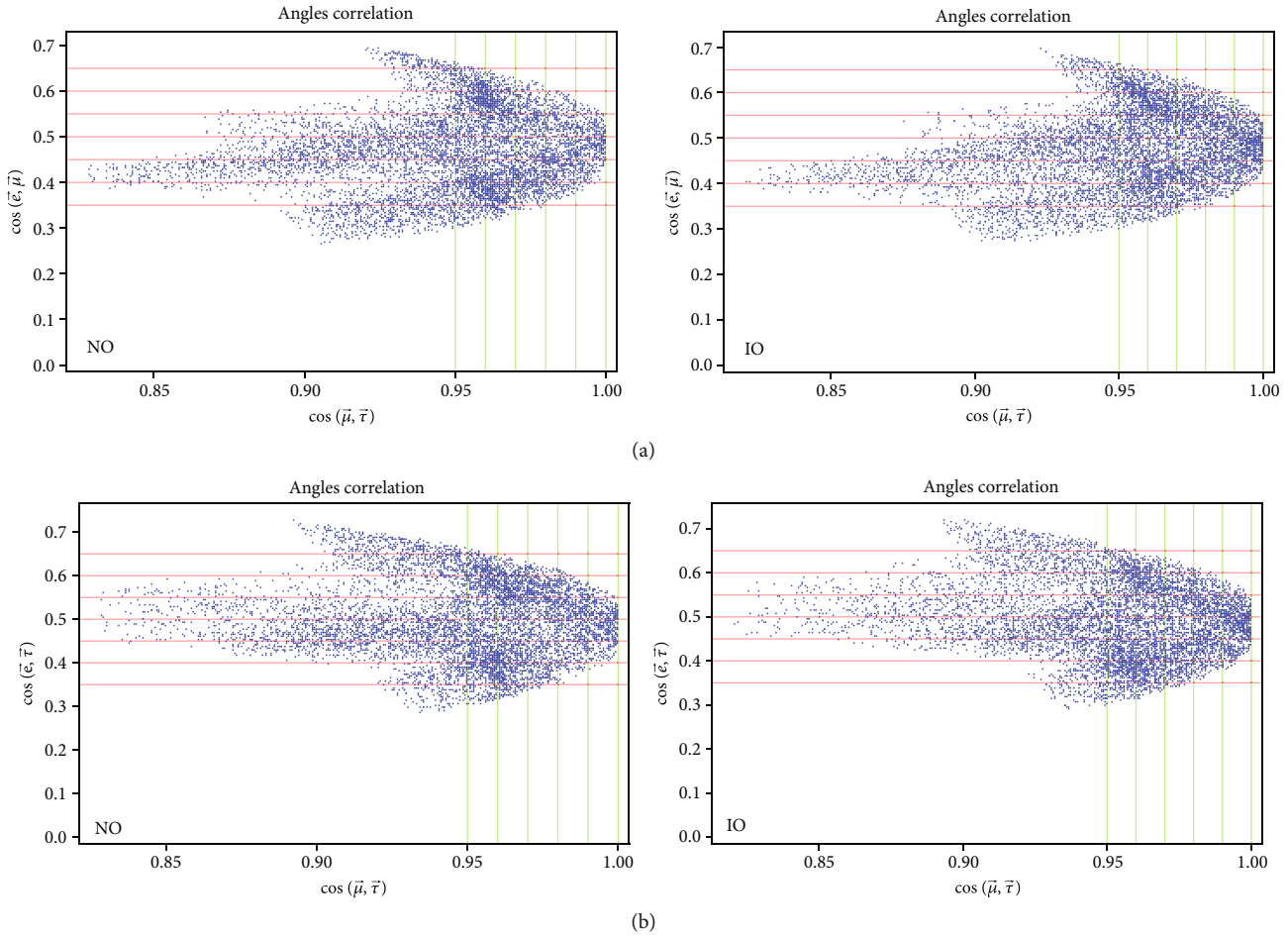

Figure 2: (a) Front view. (b) Top view.

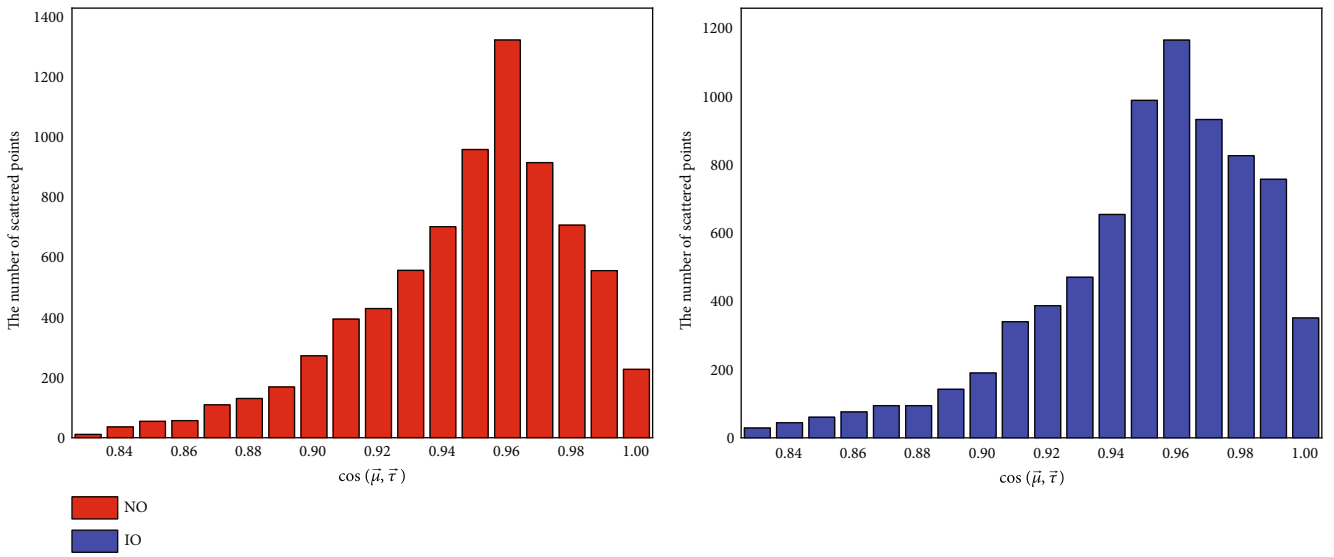

Figure 3: The number of scattered points corresponding to a series of small intervals of cos $(\vec{\mu}, \vec{\tau})$ in Figure 2. Red: NO case. Blue: IO case.

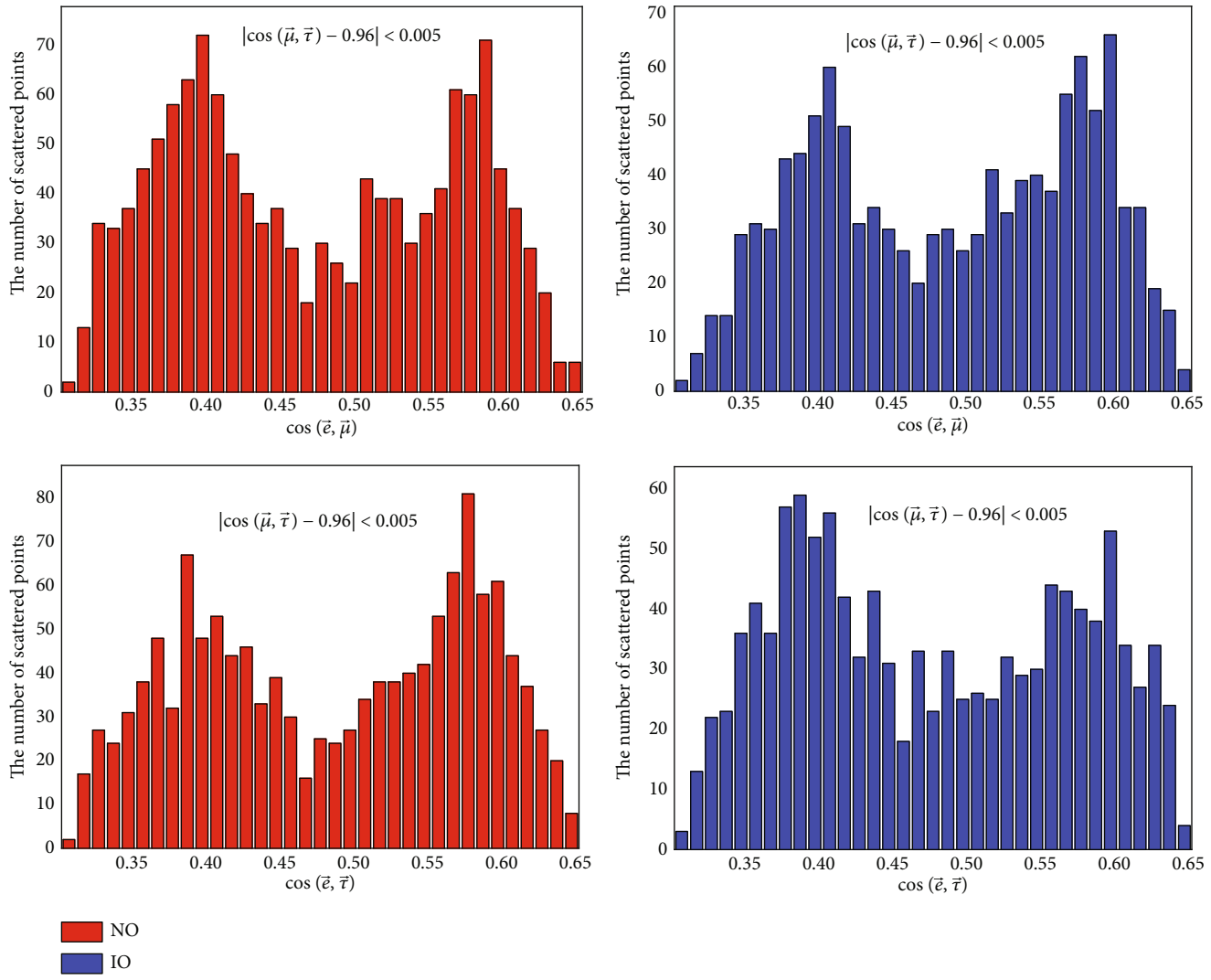

Figure 4: The number of scattered points corresponding to a series of small intervals of $\cos(\vec{e},\vec{\mu})$ and $\cos(\vec{e},\vec{\tau})$ in Figure 2, with the constraint of $|\cos(\vec{\mu},\vec{\tau}) - 0.96| < 0.005$. Red: NO case. Blue: IO case.

the largest number of scattered points in every dense area of Figure 2.

In addition, the approximated $\mu - \tau$ reflection symmetry corresponding to one of the dense regions in the IO case should be considered. In this case, the number of scattered points of $\cos(\vec{e},\vec{\mu})$ and $\cos(\vec{e},\vec{\tau})$ is shown in Figure 5, with the constraint of $0.995 < \cos(\vec{\mu},\vec{\tau}) < 1.00$.

From Figure 5, we find that the largest number of scattered points corresponds to the intervals $|\cos(\vec{e},\vec{\mu}) - 0.49| < 0.005$ and $|\cos(\vec{e},\vec{\tau}) - 0.48| < 0.005$.

On the basis of the above analysis, the selected representative intervals of the angles between the row vectors are listed in Table 2.

Now, we show that the difference on the correlations of the lepton mixing parameters from two arbitrary data points in the same interval of Figures 3–5 can be ignored. For specific explanation, three intervals in the NO case listed in Table 2 are taken, which are listed as follows: $\cos(\vec{\mu},\vec{\tau}) \in [0.955, 0.965]$, $\cos(\vec{e},\vec{\mu}) \in [0.395, 0.405]$, and $\cos(\vec{e},\vec{\tau}) \in [0.385, 0.395]$. We set constraints on the leptonic mixing parameters with small neighborhoods around the data points, which are expressed as

$$\begin{aligned} \left|\cos\left(\vec{\mu},\vec{\tau}\right) - f_1\right| &< 0.001, \\ \left|\cos\left(\vec{\mu},\vec{\tau}\right) - f_2\right| &< 0.001, \end{aligned} \tag{3}$$

$$\begin{aligned} \left|\cos\left(\vec{e},\vec{\mu}\right) - g_1\right| &< 0.001, \\ \left|\cos\left(\vec{e},\vec{\mu}\right) - g_2\right| &< 0.001, \end{aligned} \tag{4}$$

$$\begin{aligned} \left|\cos\left(\vec{e},\vec{\tau}\right) - h_1\right| &< 0.001, \\ \left|\cos\left(\vec{e},\vec{\tau}\right) - h_2\right| &< 0.001, \end{aligned} \tag{5}$$

where $(f_1 = 0.956, f_2 = 0.964)$, $(g_1 = 0.396, g_2 = 0.404)$, and $(h_1 = 0.386, h_2 = 0.394)$ are two data points near the

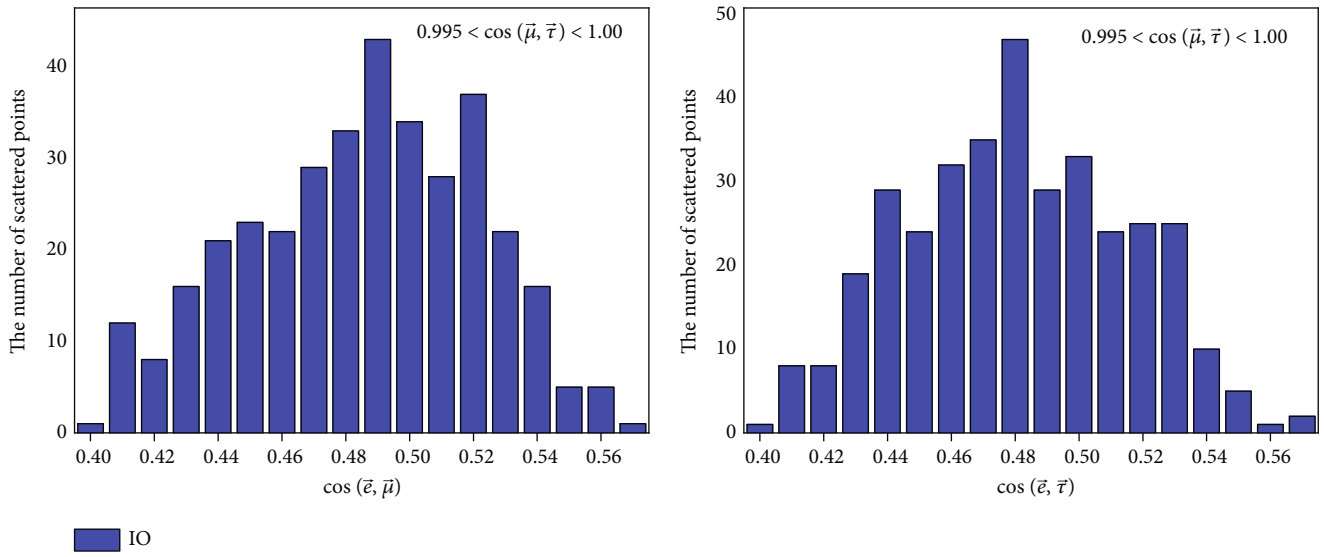

Figure 5: The number of scattered points corresponding to a series of small intervals of cos $(\vec{e}, \vec{\mu})$ and cos $(\vec{e}, \vec{\tau})$ in the IO case of Figure 2, with the constraint of $0.995 < \cos(\vec{\mu}, \vec{\tau}) < 1.00$.

Table 2: The intervals of the angles between the row vectors with the largest number of scattered points stem from every dense regions of Figure 2.

Mass ordering	$\cos\left(\vec{\mu}, \vec{\tau}\right)$	$\cos\left(\vec{e}, \vec{\mu}\right)$	$\cos\left(\vec{e}, \vec{\tau}\right)$
NO	[0.955, 0.965]	[0.395, 0.405]	[0.385, 0.395]
	[0.955, 0.965]	[0.585, 0.595]	[0.575, 0.585]
IO	[0.955, 0.965]	[0.405, 0.415]	[0.385, 0.395]
	[0.955, 0.965]	[0.595, 0.605]	[0.595, 0.605]
	[0.995, 1.00]	[0.485, 0.495]	[0.475, 0.485]

boundary of the intervals [0.955, 0.965], [0.395, 0.405], and [0.385, 0.395], respectively. The correlations of $\sin^2\theta_{23}$-δ from the above constraints are obtained at the 3σ level of the global fit data [43], which are shown in Figure 6.

Here, the correlations of $\sin^2\theta_{13}$-$\sin^2\theta_{12}$ from the constrains of Equations (3)–(5) are not given because they are insensitive to these constrains. In other words, the data points of the correlation of $\sin^2\theta_{13}$-$\sin^2\theta_{12}$ are of a uniform distribution at the 3σ level. From Figure 6, we can see that the scattered point distribution of the correlation is not sensitive to the representative points in the interval. Therefore, we choose the middle point as the representative of an interval. For the selected intervals listed in Table 2, the typical points are given in Table 3.

2.3. Leptonic Mixing Parameters Constrained by the Geometric Correlations. Now, we analyse the impacts of the geometric correlations on the leptonic mixing patterns.

2.3.1. Impacts of the Correlations of Two Included Angles. According to the typical points shown in Table 3, 15 viable correlations of two angles between the row vectors are obtained at the 3σ level of the global fit data [43], which are listed in Table 4.

Employing the correlations of the included angles in Table 4, we set the geometric constraints as follows:

$$\begin{cases} \left|\cos\left(\vec{\mu}, \vec{\tau}\right) - \cos\left(\vec{\mu_0}, \vec{\tau_0}\right)\right| < 0.001, \\ \left|\cos\left(\vec{e}, \vec{\mu}\right) - \cos\left(\vec{e_0}, \vec{\mu_0}\right)\right| < 0.001, \end{cases} \\ \begin{cases} \left|\cos\left(\vec{\mu}, \vec{\tau}\right) - \cos\left(\vec{\mu_0}, \vec{\tau_0}\right)\right| < 0.001, \\ \left|\cos\left(\vec{e}, \vec{\tau}\right) - \cos\left(\vec{e_0}, \vec{\tau_0}\right)\right| < 0.001, \end{cases} \\ \begin{cases} \left|\cos\left(\vec{e}, \vec{\mu}\right) - \cos\left(\vec{e_0}, \vec{\mu_0}\right)\right| < 0.001, \\ \left|\cos\left(\vec{e}, \vec{\tau}\right) - \cos\left(\vec{e_0}, \vec{\tau_0}\right)\right| < 0.001. \end{cases} \tag{6}$$

On the bases of the constraints, the correlations between the leptonic mixing parameters are shown in Figures 7–9.

Since the figure in the IO case is similar to the counterpart in the NO case, the plots of correlations in the IO case except the plots for the approximated $\mu - \tau$ symmetry are not shown here. We make some comments on the main observations as follows:

(a) The range of $\sin^2\theta_{12}$ is obviously reduced by the constraint of $(\cos(\vec{e_0}, \vec{\mu_0}), \cos(\vec{e_0}, \vec{\tau_0}))$ (see Figure 9). In contrast, the influence of the constraints of $(\cos(\vec{\mu_0}, \vec{\tau_0}), \cos(\vec{e_0}, \vec{\mu_0}))$ and $(\cos(\vec{\mu_0}, \vec{\tau_0}), \cos(\vec{e_0}, \vec{\tau_0}))$ on the range of $\sin^2\theta_{12}$ can be neglected

(b) δ and $\sin^2\theta_{23}$ are sensitive to the constraint of $(\cos(\vec{\mu_0}, \vec{\tau_0}), \cos(\vec{e_0}, \vec{\mu_0}))$ and/or $(\cos(\vec{\mu_0}, \vec{\tau_0}), \cos(\vec{e_0}, \vec{\tau_0}))$; that is, the ranges of the parameters are compressed apparently

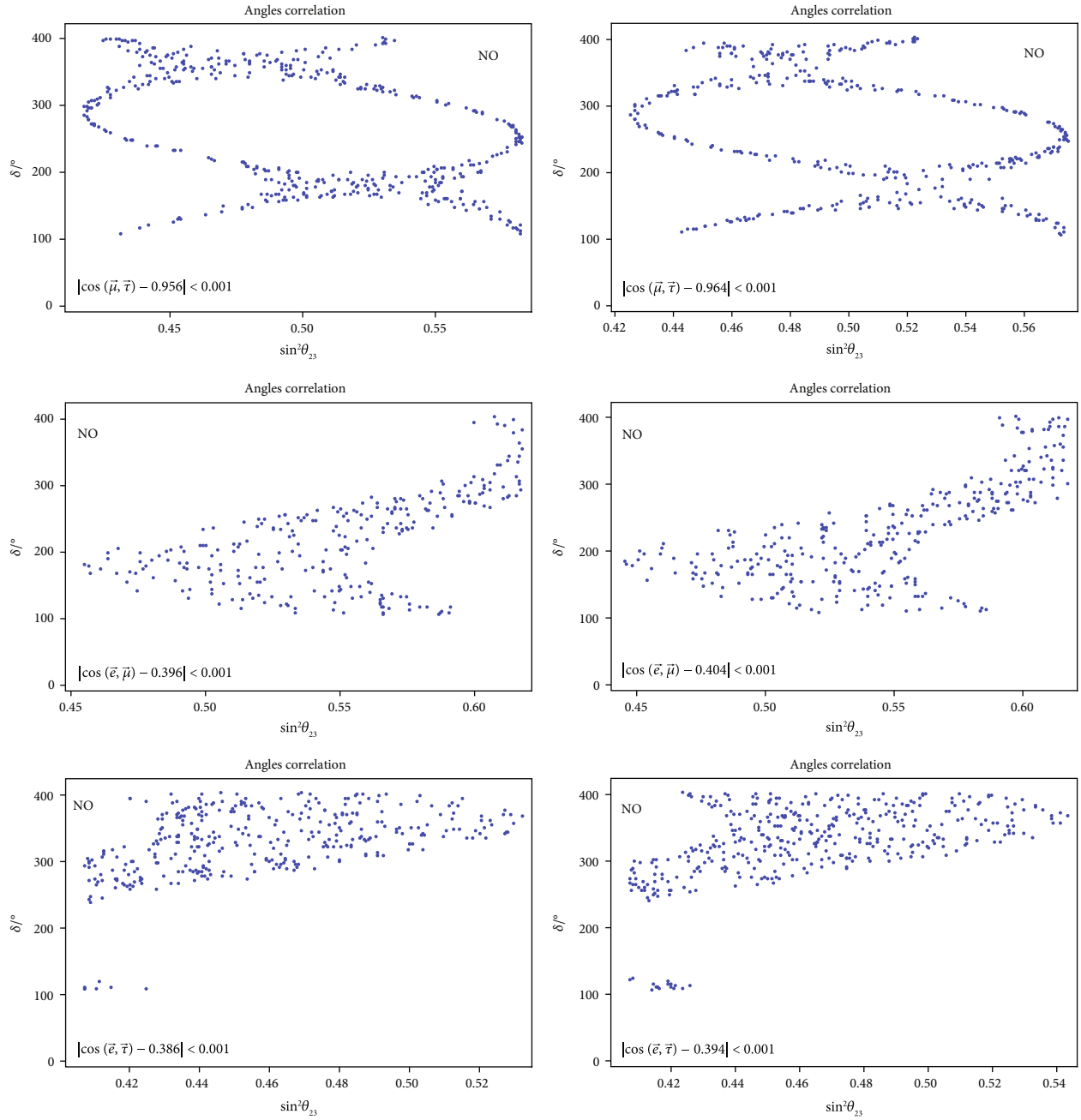

Figure 6: The correlations of $\sin^2\theta_{23}$-δ constrained by the correlations of Equations (3)–(5) at the 3σ level of the global fit data [43].

Table 3: Typical data points in the dense regions of Figure 2.

Mass ordering	$\cos(\vec{\mu_0},\vec{\tau_0})$	$\cos(\vec{e_0},\vec{\mu_0})$	$\cos(\vec{e_0},\vec{\tau_0})$
NO	0.96	0.40, 0.59	0.39, 0.58
IO	0.96	0.41, 0.60	0.39, 0.60
	0.997	0.49	0.48

(c) The above observations are stable under the variation of the intensity of the constraint, such as $|\cos(\vec{\alpha},\vec{\beta}) - \cos(\vec{\alpha_0},\vec{\beta_0})| < 0.001 \longrightarrow |\cos(\vec{\alpha},\vec{\beta}) - \cos(\vec{\alpha_0},\vec{\beta_0})| < 0.02$ with $\alpha, \beta = e, \mu, \tau$

(d) The correlations $(\cos(\vec{\mu_0},\vec{\tau_0}), \cos(\vec{e_0},\vec{\mu_0})) = (0.96, 0.40)$ and $(\cos(\vec{\mu_0},\vec{\tau_0}), \cos(\vec{e_0},\vec{\mu_0})) = (0.96, 0.59)$ can be converted to each other through the approximated $\mu - \tau$ interchange, which means that $\theta_{23} \longrightarrow \pi/2 - \theta_{23}$ and $\delta \longrightarrow \delta + \pi$. This conclusion also applies to the correlations $(\cos(\vec{\mu_0},\vec{\tau_0}), \cos(\vec{e_0},\vec{\tau_0})) = (0.96, 0.39)$ and $(\cos(\vec{\mu_0},\vec{\tau_0}), \cos(\vec{e_0},\vec{\tau_0})) = (0.96, 0.58)$ and the correlations $(\cos(\vec{e_0},\vec{\mu_0}), \cos(\vec{e_0},\vec{\tau_0})) = (0.40, 0.58)$ and $(\cos(\vec{e_0},\vec{\mu_0}), \cos(\vec{e_0},\vec{\tau_0})) = (0.59, 0.39)$

Table 4: Viable combinations with two included angles of the row vectors.

Mass ordering	$(\cos(\overrightarrow{\mu_0}, \overrightarrow{\tau_0}), \cos(\overrightarrow{e_0}, \overrightarrow{\mu_0}))$	$(\cos(\overrightarrow{\mu_0}, \overrightarrow{\tau_0}), \cos(\overrightarrow{e_0}, \overrightarrow{\tau_0}))$	$(\cos(\overrightarrow{e_0}, \overrightarrow{\mu_0}), \cos(\overrightarrow{e_0}, \overrightarrow{\tau_0}))$
NO	(0.96, 0.40)	(0.96, 0.39)	(0.40, 0.58)
	(0.96, 0.59)	(0.96, 0.58)	(0.59, 0.39)
IO	(0.96, 0.41)	(0.96, 0.39)	(0.41, 0.60)
	(0.96, 0.60)	(0.96, 0.60)	(0.60, 0.39)
	(0.997, 0.49)	(0.997, 0.48)	(0.49, 0.48)

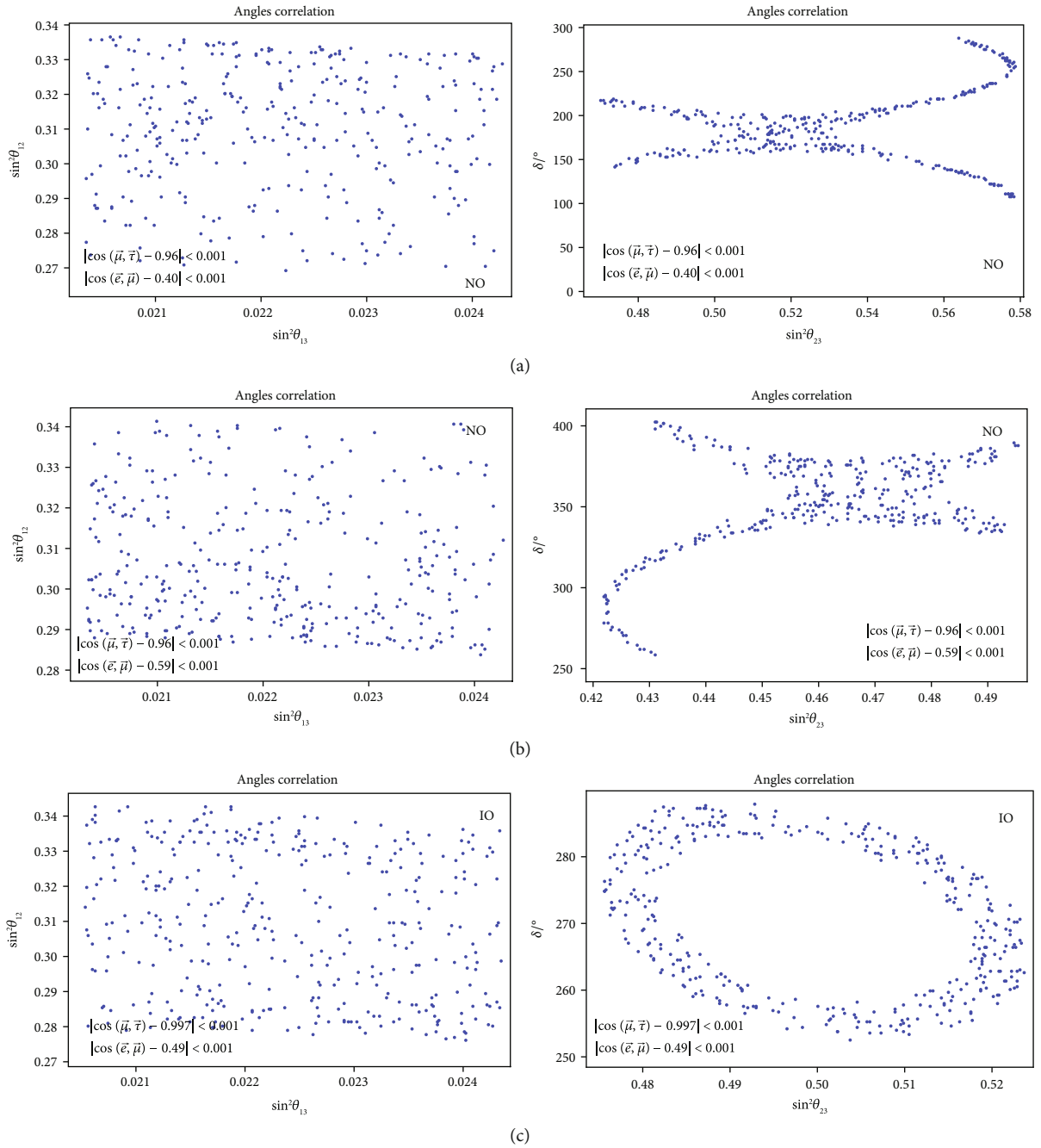

Figure 7: Leptonic mixing parameters constrained by the correlations between two included angles of $(\cos(\overrightarrow{\mu_0}, \overrightarrow{\tau_0}), \cos(\overrightarrow{e_0}, \overrightarrow{\mu_0}))$ listed in Table 4. (a) NO case with the constraints of $|\cos(\vec{\mu}, \vec{\tau}) - 0.96| < 0.001$ and $|\cos(\vec{e}, \vec{\mu}) - 0.40| < 0.001$. (b) NO case with the constraints of $|\cos(\vec{\mu}, \vec{\tau}) - 0.96| < 0.001$ and $|\cos(\vec{e}, \vec{\mu}) - 0.59| < 0.001$. (c) IO case with the constraints of $|\cos(\vec{\mu}, \vec{\tau}) - 0.997| < 0.001$ and $|\cos(\vec{e}, \vec{\mu}) - 0.49| < 0.001$.

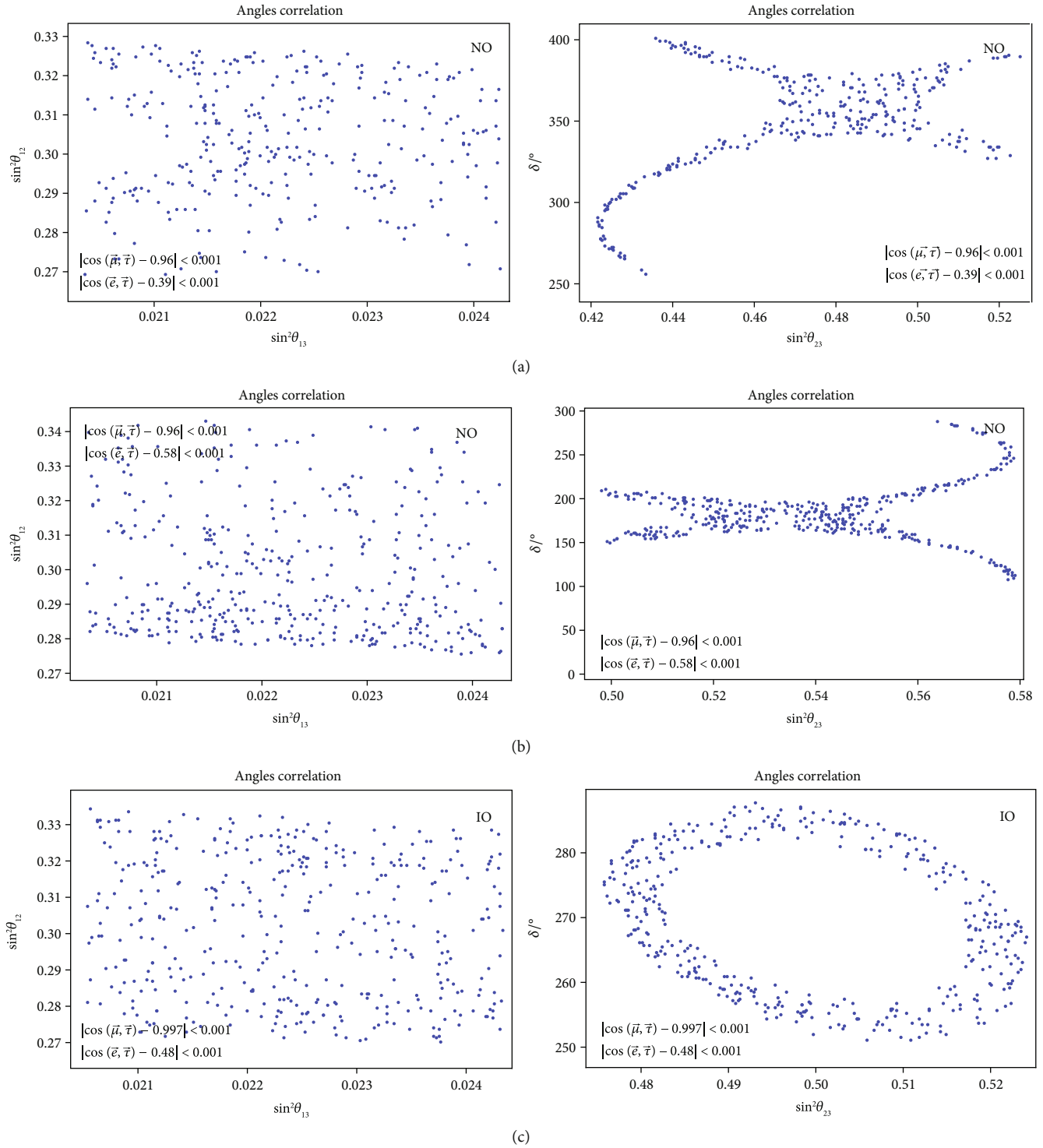

FIGURE 8: Leptonic mixing parameters constrained by the correlations between two included angles of $(\cos(\vec{\mu_0},\vec{\tau_0}),\cos(\vec{e_0},\vec{\tau_0}))$ listed in Table 4. (a) NO case with the constraints of $|\cos(\vec{\mu},\vec{\tau})-0.96|<0.001$ and $|\cos(\vec{e},\vec{\tau})-0.39|<0.001$. (b) NO case with the constraints of $|\cos(\vec{\mu},\vec{\tau})-0.96|<0.001$ and $|\cos(\vec{e},\vec{\tau})-0.58|<0.001$. (c) IO case with the constraints of $|\cos(\vec{\mu},\vec{\tau})-0.997|<0.001$ and $|\cos(\vec{e},\vec{\tau})-0.48|<0.001$.

(e) The correlation of the leptonic mixing parameters obtained from the correlation $(\cos(\vec{\mu_0},\vec{\tau_0}),\cos(\vec{e_0},\vec{\mu_0}))=(0.96,0.40)$ is similar as that obtained from the correlation $(\cos(\vec{\mu_0},\vec{\tau_0}),\cos(\vec{e_0},\vec{\tau_0}))=(0.96,0.58)$. The difference of these two correlations is that the range of $\sin^2\theta_{23}$ from the latter is moderately

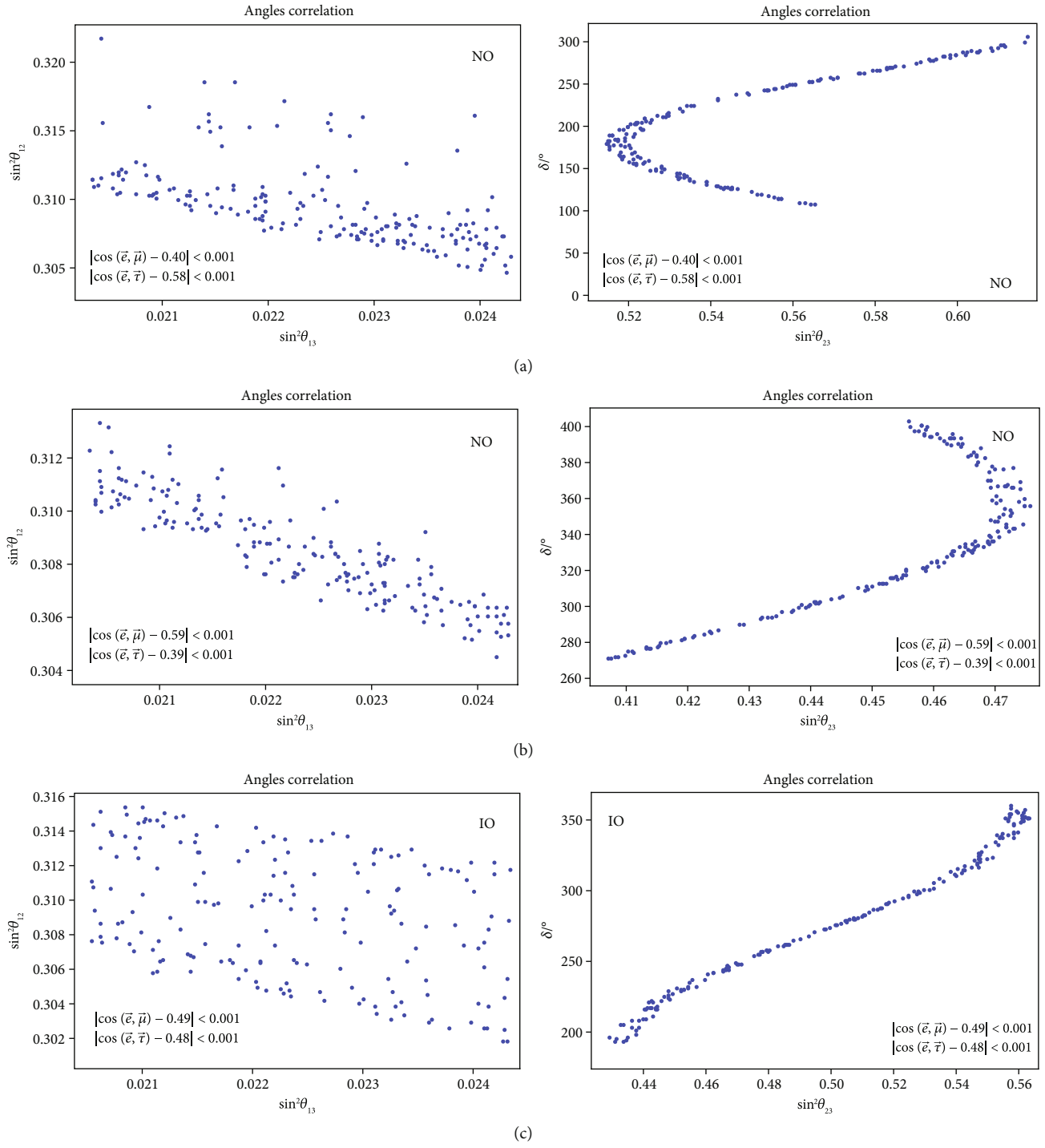

Figure 9: Leptonic mixing parameters constrained by the correlations between two included angles of $(\cos(\vec{e_0},\vec{\mu_0}),\cos(\vec{e_0},\vec{\tau_0}))$ listed in Table 4. (a) NO case with the constraints of $|\cos(\vec{e},\vec{\mu})-0.40|<0.001$ and $|\cos(\vec{e},\vec{\tau})-0.58|<0.001$. (b) NO case with the constraints of $|\cos(\vec{e},\vec{\mu})-0.59|<0.001$ and $|\cos(\vec{e},\vec{\tau})-0.39|<0.001$. (c) IO case with the constraints of $|\cos(\vec{e},\vec{\mu})-0.49|<0.001$ and $|\cos(\vec{e},\vec{\tau})-0.48|<0.001$.

compressed. This observation also applies to the correlations $(\cos(\vec{\mu_0},\vec{\tau_0}),\cos(\vec{e_0},\vec{\mu_0}))=(0.96,0.59)$ and $(\cos(\vec{\mu_0},\vec{\tau_0}),\cos(\vec{e_0},\vec{\tau_0}))=(0.96,0.39)$

2.3.2. Leptonic Mixing Parameters Constrained by Correlations of Three Included Angles. According to the observations in the case of the correlations of two included angles, we find that the mixing parameters ($\sin^2\theta_{12}$, $\sin^2\theta_{23}$, and δ) are strictly constrained by the geometric correlations. Now, we extract the correlations between the mixing parameters from the correlations of three included angles.

Table 5: Representative correlations of three included angles.

Mass ordering	Correlations	$\left(\cos\left(\overrightarrow{\mu_0},\overrightarrow{\tau_0}\right),\cos\left(\overrightarrow{e_0},\overrightarrow{\mu_0}\right),\cos\left(\overrightarrow{e_0},\overrightarrow{\tau_0}\right)\right)$
NO	I	(0.96, 0.40, 0.58)
	II	(0.96, 0.59, 0.39)
IO	III	(0.96, 0.41, 0.60)
	IV	(0.96, 0.60, 0.39)
	V	(0.997, 0.49, 0.48)

On the basis Tables 3, 5 correlations of three included angles are viable at the 3σ level of the global fit data [43], which are listed in Table 5.

Employing the geometric constraints listed as follows:

$$\begin{cases} \left|\cos\left(\vec{\mu},\vec{\tau}\right)-\cos\left(\overrightarrow{\mu_0},\overrightarrow{\tau_0}\right)\right|<0.001, \\ \left|\cos\left(\vec{e},\vec{\mu}\right)-\cos\left(\overrightarrow{e_0},\overrightarrow{\mu_0}\right)\right|<0.001, \\ \left|\cos\left(\vec{e},\vec{\tau}\right)-\cos\left(\overrightarrow{e_0},\overrightarrow{\tau_0}\right)\right|<0.001, \end{cases} \tag{7}$$

we get the correlations of the leptonic mixing parameters, shown in Figure 10.

From Figure 10, we obtain the following observations:

(a) $\sin^2\theta_{12}$ is linearly dependent on $\sin^2\theta_{13}$ for all the correlations and is consistent with the recent global best fit value [43] under the correlation V. Correspondingly, the range of $\sin^2\theta_{12}$ is reduced significantly by the geometric constraints. Furthermore, under the constraint intensity, namely, 10^{-3}, the variation of $\sin^2\theta_{12}$ is at most 2×10^{-3}. Therefore, the breaking of the $\mu-\tau$ reflection symmetry is mainly determined by the included angles, i.e., $\cos\left(\overrightarrow{\alpha_0},\overrightarrow{\beta_0}\right)$ with $\alpha,\beta=e,\mu,\tau$

(b) The range of $\sin^2\theta_{23}$ displays two branches for all the correlations. The right branch of $\sin^2\theta_{23}$ from the correlation III is consistent with the recent global best fit value [43], while the left branch of $\sin^2\theta_{23}$ from correlation III is consistent with the best fit value of T2K experiment ($\sin^2\theta_{23}=0.53^{+0.03}_{-0.04}$) [44]

(c) The range of δ also presents two branches for the correlations I-V. The best global fit value of δ in the NO case [43] can be realized from the correlation I, and the value in the IO case can be obtained from the correlations IV and V

(d) The correlations I and II can be converted to each other through the approximated $\mu-\tau$ interchange

(e) We note that the values of $\sin^2\theta_{12}$, $\sin^2\theta_{13}$, $\sin^2\theta_{23}$, and δ predicted from the modular symmetry origin of texture zeros and quark-lepton unification (see models III+$\mathscr{D}_6$ and IV+$\mathscr{D}_6$ in the Ref. [45]) are close to the ones shown in the special branch from the correlation I in the top plots of Figure 10. In addition, the values of the mixing angles and the Dirac CP phase predicted from the A_5' modular group (see lepton models $\mathscr{L}_{134}$, $\mathscr{L}_3$, and $\mathscr{L}_{10}$ in the Ref. [46]) also approach to the ones in the branch from the correlation I in Figure 10. Thus, the geometric correlations may be realized in the lepton mixing models based on modular symmetries

3. The Flavor Ratio of High-Energy Astronomical Neutrinos

In the previous section, we studied the geometric correlations and the corresponding leptonic mixing parameters. Now, we show the implications of geometric correlations on neutrino phenomenology. As a specific example, we discuss the impacts of geometric correlations on the flavor ratio of HANs at Earth in this section.

In recent years, a number of HAN events have been detected by the IceCube Collaboration in the energy range of TeV-PeV [47–50]. These neutrinos traveled long distances of the cosmological scale. Their flavor transition probability $\bar{P}_{\alpha\beta}$ in the standard framework is expressed as

$$\bar{P}_{\alpha\beta}=|U_{\alpha1}|^2\left|U_{\beta1}\right|^2+|U_{\alpha2}|^2\left|U_{\beta2}\right|^2+|U_{\alpha3}|^2\left|U_{\beta3}\right|^2, \tag{8}$$

where $\alpha,\beta=e,\mu,\tau$ and $U_{\alpha i}(i=1,2,3)$ is the element of the PMNS matrix. Using the flavor conversion matrix $\bar{P}$ and the flavor composition at the source of HANs, we can derive the flavor ratio at Earth, i.e., $\Phi^E=\bar{P}\Phi^S$. Here, Φ^S and Φ^E denote the flavor ratio at the source and that at Earth, respectively. Since neither matter effects nor new physics effects are in favor of neutron decay as the sole source of the HANs [51, 52], we take into account two typical sources in this paper, namely,

$$\begin{aligned} &\text{muon-damping source with } \Phi^S=(0,1,0)^T, \\ &\text{pion-decay source with } \Phi^S=(1/3,2/3,0)^T. \end{aligned} \tag{9}$$

For a given source, the uncertainty of the predicted flavor ratio at Earth is large due to the imprecise leptonic mixing parameters. As is known, the constraints of geometric correlations can significantly reduce the ranges of the leptonic mixing parameters. Accordingly, the precision of Φ^E can be notably improved. Here, we show the impacts of the representative geometric correlations on Φ^E in Figures 11–13. For the sake of comparison, the flavor ratio predicted with the leptonic mixing parameters at the 3σ level of the global fit data [43] and those constrained by the $\mu-\tau$ reflection symmetry are also shown in the ternary plots.

From these figures, we obtain the following observations:

(a) For both sources of HANs, the uncertainty of the predicted flavor ratio at Earth is obviously decreased by the geometrical constraints of every correlation.

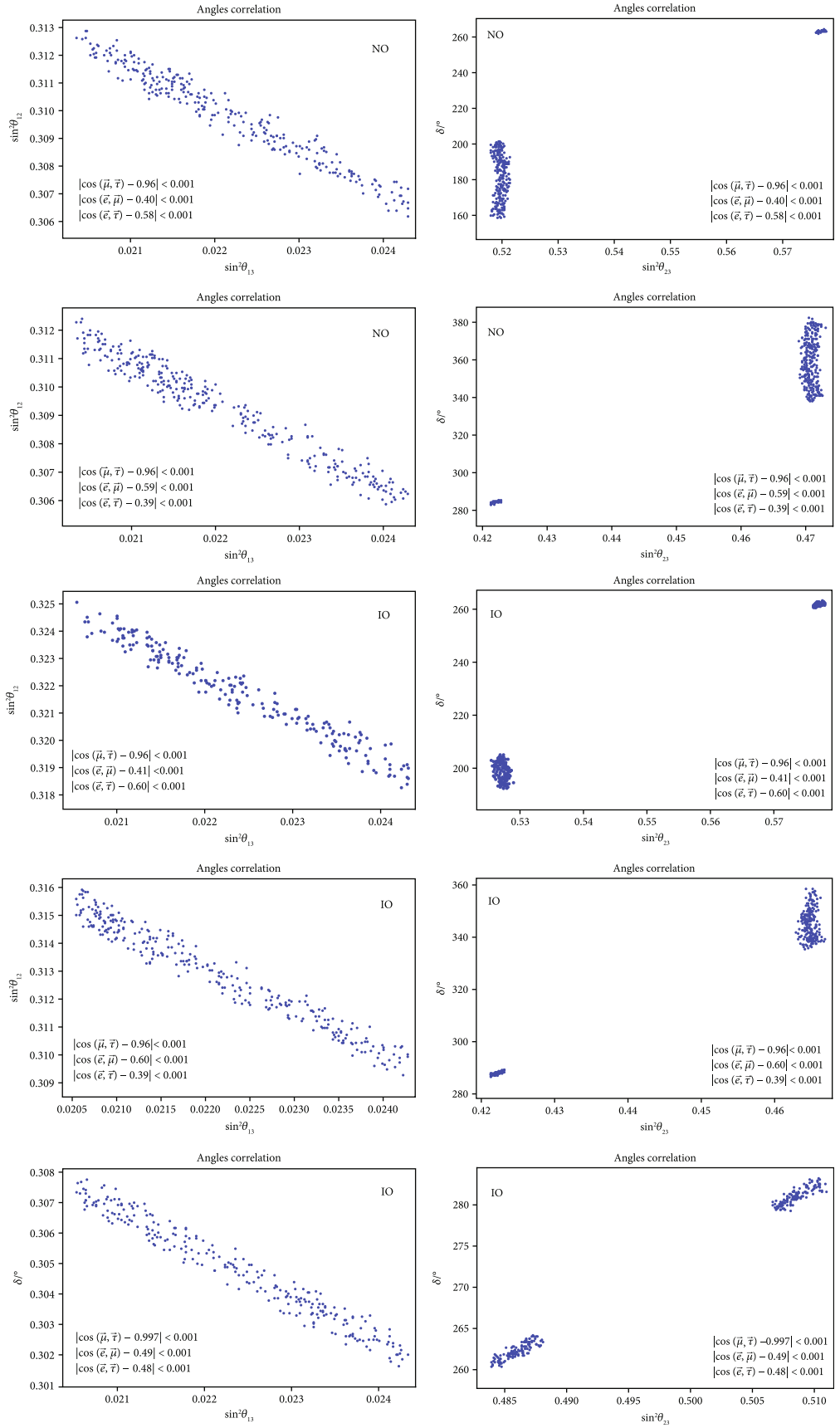

FIGURE 10: The correlations of $\sin^2\theta_{13}$-$\sin^2\theta_{12}$ and $\sin^2\theta_{23}$-δ from the constraints of the geometric correlations I-V.

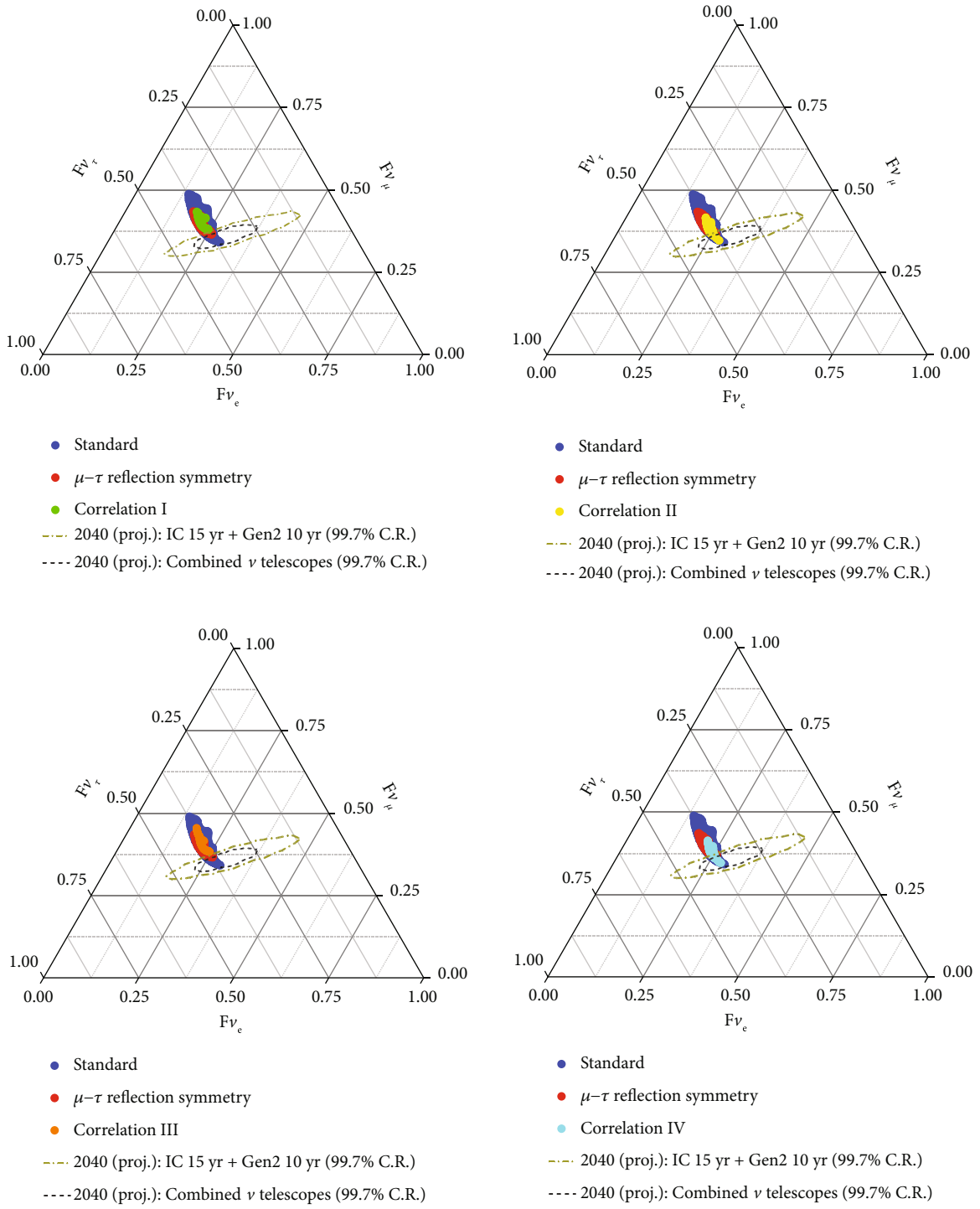

FIGURE 11: Ternary plot of the flavor ratio at Earth with the muon-damping decay source. "Standard" denotes the flavor ratio predicted with the leptonic mixing parameters at the 3σ level of the global fit data [43]. "$\mu-\tau$ reflection symmetry" denotes the flavor composition that adds a constrain of $|\cos(\vec{\mu},\vec{\tau})-1|<0.001$ to the "standard" case. The geometric constraints of correlations I-IV are defined in Table 5 and Equation (7). The 2040 3σ credible region with the pion-decay source based on IceCube and IceCube-Gen2 is taken from Ref. [53]. The 3σ credible region with the pion-decay source based on all TeV-PeV neutrino telescopes available in 2040 is taken from Ref. [54].

In contrast to the strict $\mu-\tau$ reflection symmetry, the geometrical correlations have more notable impacts on the predicted flavor ratio

(b) For the muon-damping source (Figures 11 and 13(a)), the predicted flavor ratio constrained by the correlation I and/or III is outside the 3σ credible

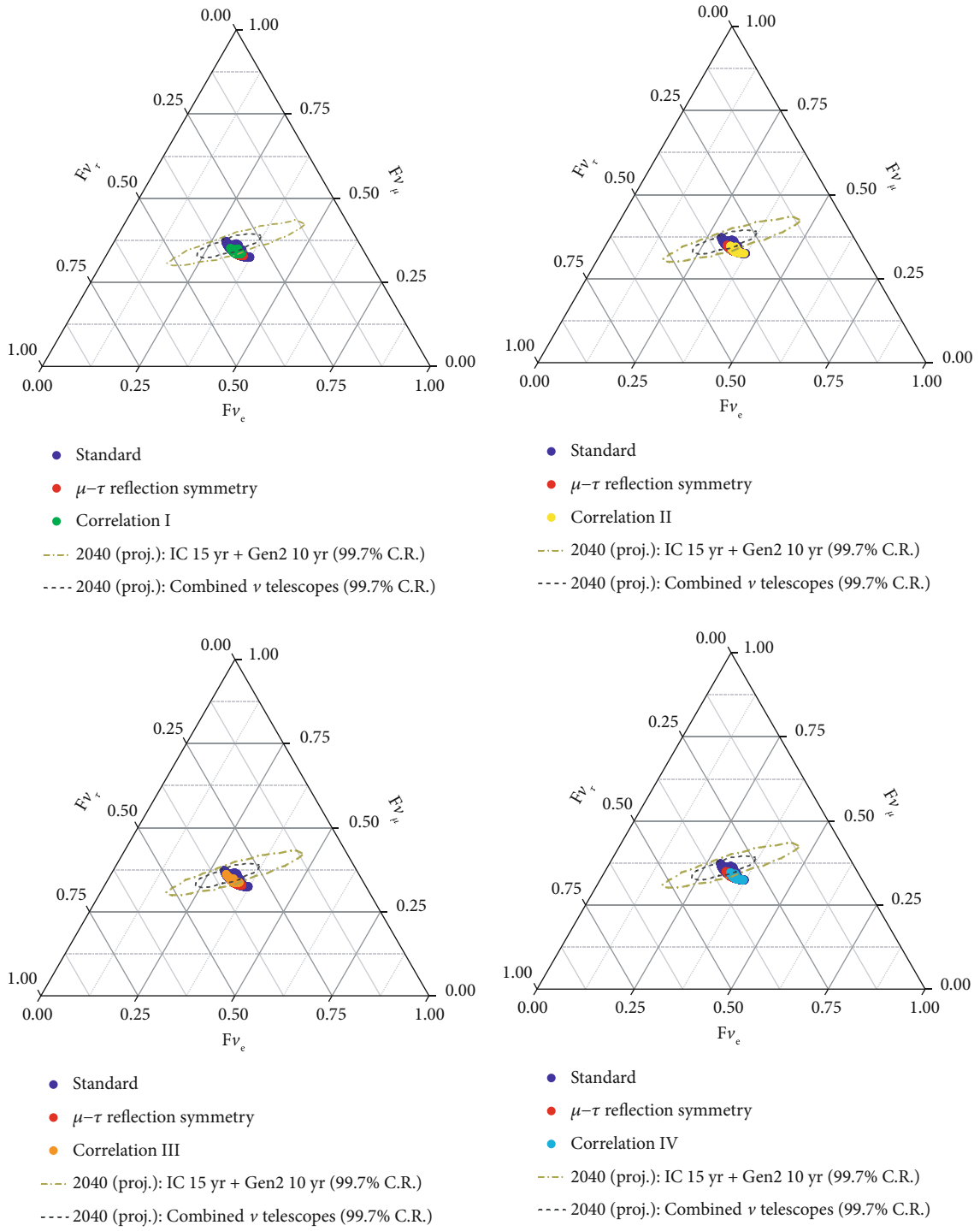

Figure 12: Ternary plot of the flavor ratio at Earth with the pion-decay source based on the geometric constraints of the correlations I-IV. The conventions of parameters and colors are the same as those in Figure 11.

region with the pion-decay source based on all neutrino telescopes [54]. However, a small part of the flavor ratio at Earth, which constrained by the correlation II, IV, and/or V falls into the 3σ credible region with the pion-decay source. Therefore, with the help of geometrical correlations, the muon-damping decay source may be discriminated from the pion-decay source in the near future

(c) For the pion-decay source (Figures 12 and 13(b)), the primary part of the flavor ratio constrained by the correlation II and/or IV is outside the 2040 3σ

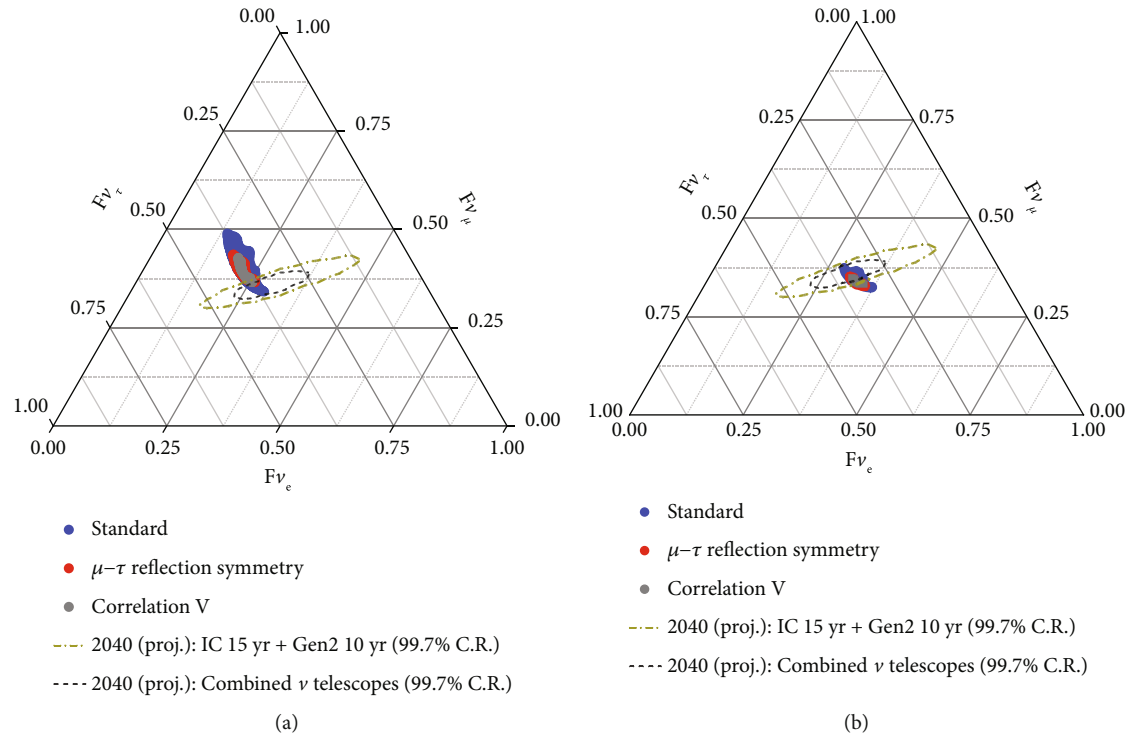

Figure 13: Ternary plot of the flavor ratio at Earth with the muon-damping decay source (a) and the pion-decay source (b) based on the geometric constraints of the correlation V. The conventions of parameters and colors are the same as those in Figure 11.

credible region. Thus, the correlations II and IV with this source would be stringently constrained by the observations of the neutrino telescopes in the future

4. Conclusions

The $\mu - \tau$ reflection symmetry has been proposed for twenty years. Its prediction still satisfies the constraints of the recent global fit data of neutrino oscillations. From the geometric perspective, this symmetry and its breaking can be represented by the angles between the row vectors of the magnitude of the leptonic mixing matrix. Employing the geometric quantities, we studied the promising correlations between the leptonic mixing parameters. On the bases of the mixing parameters constrained by the geometric correlations, the flavor ratio of HANs at Earth with typical sources has been discussed. Our main results are summarized as follows.

First, the data points of the included angles of the row vectors are concentrated on several special regions in the scattered plots. In the IO case, one of the regions corresponds to the approximated $\mu - \tau$ reflection symmetry. From other regions, promising correlations of leptonic mixing parameters are read out.

Second, we find that $\sin^2\theta_{12}$ is sensitive to the correlation $(\cos(\overrightarrow{e_0}, \overrightarrow{\mu_0}), \cos(\overrightarrow{e_0}, \overrightarrow{\tau_0}))$ in both the NO case and IO case. In contrast, $\sin^2\theta_{23}$ and δ change notably under the moderate variation of the correlations $(\cos(\overrightarrow{\mu_0}, \overrightarrow{\tau_0}), \cos(\overrightarrow{e_0}, \overrightarrow{\mu_0}))$ and/or $(\cos(\overrightarrow{\mu_0}, \overrightarrow{\tau_0}), \cos(\overrightarrow{e_0}, \overrightarrow{\tau_0}))$. Furthermore, the ranges of $\sin^2\theta_{23}$ and δ display disconnected branches. Thus, the included angles of the row vectors can serve as sensitive indexes of the leptonic mixing pattern to test by the neutrino oscillation experiments in future.

Third, when the correlation of the three included angles $(\cos(\overrightarrow{e_0}, \overrightarrow{\mu_0}), \cos(\overrightarrow{e_0}, \overrightarrow{\tau_0}), \cos(\overrightarrow{\mu_0}, \overrightarrow{\tau_0}))$ is given, $\sin^2\theta_{12}$ is linearly dependent on $\sin^2\theta_{13}$, and $\sin^2\theta_{23}$ and δ can take discrete values. Hence, the uncertainties of the leptonic mixing are remarkably decreased by the geometric correlations. Correspondingly, the prediction of the flavor ratio of HANs at Earth with typical sources is notably improved. With the help of the special correlations, the discrimination of the sources may be available in the near future.

Data Availability

The data supporting this research paper are from previously reported studies, which have been cited. The processed data are freely available.

Disclosure

An arXiv has previously been published [55].

Conflicts of Interest

The authors declare that they have no conflicts of interest.

Acknowledgments

This work is supported by the National Natural Science Foundation of China under grant No. 12065007, the Guangxi

Scientific Program Foundation under grant No. Guike AD19110045, and the Research Foundation of Guilin University of Technology under grant No. GUTQDJJ2018103.

References

[1] Y. Fukuda, T. Hayakawa, E. Ichihara et al., "Evidence for oscillation of atmospheric neutrinos," *Physical review letters*, vol. 81, no. 8, p. 1562, 1998.

[2] Q. R. Ahmad, R. C. Allen, T. C. Andersen et al., "Direct evidence for neutrino flavor transformation from neutral-current interactions in the Sudbury Neutrino Observatory," *Physical Review Letters*, vol. 89, no. 1, article 011301, 2002.

[3] F. P. An, J. Z. Bai, A. B. Balantekin et al., "Observation of electron-antineutrino disappearance at Daya Bay," *Physical Review Letters*, vol. 108, no. 17, article 171803, 2012.

[4] V. D. Barger, S. Pakvasa, T. J. Weiler, and K. Whisnant, "Bimaximal mixing of three neutrinos," *Physics Letters B*, vol. 437, no. 1-2, pp. 107–116, 1998.

[5] P. F. Harrison, D. H. Perkins, and W. G. Scott, "Tri-bimaximal mixing and the neutrino oscillation data," *Physics Letters B*, vol. 530, no. 1-4, pp. 167–173, 2002.

[6] P. F. Harrison and W. G. Scott, "Symmetries and generalisations of tri-bimaximal neutrino mixing," *Physics Letters B*, vol. 535, no. 1-4, pp. 163–169, 2002.

[7] Y. Kajiyama, M. Raidal, and A. Strumia, "Golden ratio prediction for solar neutrino mixing," *Physical Review D*, vol. 76, no. 11, article 117301, 2007.

[8] L. L. Everett and A. J. Stuart, "Icosahedral (A_5) family symmetry and the golden ratio prediction for solar neutrino mixing," *Physical Review D*, vol. 79, no. 8, article 085005, 2009.

[9] A. Adulpravitchai, A. Blum, and W. Rodejohann, "Golden ratio prediction for solar neutrino mixing," *New Journal of Physics*, vol. 11, no. 6, article 063026, 2009.

[10] C. H. Albright, A. Dueck, and W. Rodejohann, "Possible alternatives to tri-bimaximal mixing," *European Physical Journal C: Particles and Fields*, vol. 70, no. 4, pp. 1099–1110, 2010.

[11] R. de Adelhart Toorop, F. Feruglio, and C. Hagedorn, "Finite modular groups and lepton mixing," *Nuclear Physics B*, vol. 858, no. 3, pp. 437–467, 2012.

[12] G.-J. Ding, "TFH mixing patterns, large θ_{13} and $\Delta(96)$ flavor symmetry," *Nuclear Physics B*, vol. 862, no. 1, pp. 1–42, 2012.

[13] G. Altarelli and F. Feruglio, "Discrete flavor symmetries and models of neutrino mixing," *Reviews of Modern Physics*, vol. 82, no. 3, pp. 2701–2729, 2010.

[14] H. Ishimori, T. Kobayashi, H. Ohki, Y. Shimizu, H. Okada, and M. Tanimoto, "Non-Abelian discrete symmetries in particle physics," *Progress of Theoretical Physics Supplement*, vol. 183, pp. 1–163, 2010.

[15] S. F. King and C. Luhn, "A_4 models of tri-bimaximal-reactor mixing," *Journal of High Energy Physics*, vol. 2012, no. 3, 2012.

[16] G. Altarelli, F. Feruglio, L. Merlo, and E. Stamou, "Repressing anarchy in neutrino mass textures," *Journal of High Energy Physics*, vol. 2012, no. 11, 2012.

[17] C. S. Lam, "Determining horizontal symmetry from neutrino mixing," *Physical Review Letters*, vol. 101, no. 12, p. 121602, 2008.

[18] K. Abe, N. Abgrall, Y. Ajima et al., "Indication of electron neutrino appearance from an accelerator-produced off-axis muon neutrino beam," *Physical Review Letters*, vol. 107, no. 4, article 041801, 2011.

[19] P. Adamson, D. J. Auty, D. S. Ayres et al., "Improved search for muon-neutrino to electron-neutrino oscillations in MINOS," *Physical Review Letters*, vol. 107, no. 18, article 181802, 2011.

[20] J. K. Ahn, S. Chebotaryov, J. H. Choi et al., "Observation of reactor electron antineutrinos disappearance in the RENO experiment," *Physical Review Letters*, vol. 108, article 191802, 2012.

[21] Y. Abe and Double Chooz Collaboration, "Indication of reactor $\bar{\nu}_e$ disappearance in the double Chooz experiment," *Physical Review Letters*, vol. 108, article 131801, 2012.

[22] B. Brahmachari and A. Raychaudhuri, "Perturbative generation of θ_{13} from tribimaximal neutrino mixing," *Physical Review D*, vol. 86, no. 5, article 051302, 2012.

[23] F. Feruglio, C. Hagedorn, and R. Ziegler, "Lepton mixing parameters from discrete and CP symmetries," *Journal of High Energy Physics*, vol. 2013, no. 7, article 27, 2013.

[24] F. Feruglio, C. Hagedorn, and R. Ziegler, "A realistic pattern of lepton mixing and masses from S_4 and CP," *European Physical Journal C: Particles and Fields*, vol. 74, no. 2, p. 2753, 2014.

[25] S.-j. Rong, "Lepton mixing patterns from the group $\Sigma(36\times3)$ with a generalized CP transformation," *Physical Review D*, vol. 95, no. 7, article 076014, 2017.

[26] S.-J. Rong, "Lepton mixing patterns from $PSL_2(7)$ with a generalized CP symmetry," *Advances in High Energy Physics*, vol. 2020, Article ID 6120803, 13 pages, 2020.

[27] N. Nath, R. Srivastava, and J. W. F. Valle, "Testing generalized CP symmetries with precision studies at DUNE," *Physical Review D*, vol. 99, no. 7, article 075005, 2019.

[28] S.-J. Rong, "New partial symmetries from group algebras for lepton mixing," *Advances in High Energy Physics*, vol. 2020, Article ID 3967605, 8 pages, 2020.

[29] S.-j. Rong, "A novel mathematical construct for the family of leptonic mixing patterns," 2017, https://arxiv.org/abs/1703.09981.

[30] P. F. Harrison and W. G. Scott, "μ-τ reflection symmetry in lepton mixing and neutrino oscillations," *Physics Letters B*, vol. 547, no. 3-4, pp. 219–228, 2002.

[31] C. Duarah, "$\mu-\tau$ reflection symmetry in the standard parametrization and contributions from charged lepton sector," *Physics Letters B*, vol. 815, p. 136119, 2021.

[32] Z.-z. Xing and Z.-h. Zhao, "A review of μ-τ flavor symmetry in neutrino physics," *Reports on Progress in Physics*, vol. 79, no. 7, article 076201, 2016.

[33] G.-y. Huang and N. Nath, "RGE-induced μ-τ symmetry breaking: an analysis of the latest T2K results," *European Physical Journal C: Particles and Fields*, vol. 80, no. 10, p. 914, 2020.

[34] Z.-h. Zhao, "Renormalization group evolution induced leptogenesis in the minimal seesaw model with the trimaximal mixing and mu-tau reflection symmetry," *Journal of High Energy Physics*, vol. 11, p. 170, 2021.

[35] T. Fukuyama and Y. Mimura, "$\mu-\tau$ symmetry breaking and CP violation in the neutrino mass matrix," *Physical Review D*, vol. 102, no. 1, article 016002, 2020.

[36] M. J. S. Yang, "Interplay between exact $\mu-\tau$ reflection symmetries, four-zero texture and universal texture," *Physics Letters B*, vol. 806, p. 135483, 2020.

[37] J. Liao, N. Nath, T. Wang, and Y.-L. Zhou, "Nonstandard neutrino interactions and mu-tau reflection symmetry," *Physical Review D*, vol. 101, no. 9, article 095036, 2020.

[38] N. Chamoun, C. Hamzaoui, S. Lashin, S. Nasri, and M. Toharia, "Phase broken $\mu-\tau$ symmetry and the neutrino

mass hierarchy," *Physical Review D*, vol. 104, no. 1, article 015004, 2021.

[39] N. Nath, "Impact of RGE-induced μ–τ reflection symmetry breaking on the effective Majorana neutrino mass in $0\nu\beta\beta$ decay," *Physical Review D*, vol. 99, no. 3, article 035026, 2019.

[40] B. Pontecorvo, "Neutrino experiments and the problem of conservation of leptonic charge," *Zhurnal Eksperimental'noi i Teoreticheskoi Fiziki*, vol. 53, pp. 1717–1725, 1967.

[41] Z. Maki, M. Nakagawa, and S. Sakata, "Remarks on the unified model of elementary particles," *Progress in Theoretical Physics*, vol. 28, no. 5, pp. 870–880, 1962.

[42] P. A. Zyla, R. M. Barnett, J. Beringer et al., "Review of particle physics," *PTEP*, vol. 2020, no. article 083C01, 2020.

[43] I. Esteban, M. C. Gonzalez-Garcia, M. Maltoni, T. Schwetz, and A. Zhou, "The fate of hints: updated global analysis of three-flavor neutrino oscillations," *Journal of High Energy Physics*, vol. 2020, no. 9, article 178, 2020.

[44] The T2K Collaboration, "Constraint on the matter–antimatter symmetry-violating phase in neutrino oscillations," *Nature*, vol. 580, pp. 339–344, 2020.

[45] J.-N. Lu, X.-G. Liu, and G.-J. Ding, "Modular symmetry origin of texture zeros and quark-lepton unification," *Physical Review D*, vol. 101, no. 11, p. 115020, 2020.

[46] C.-Y. Yao, X.-G. Liu, and G.-J. Ding, "Fermion masses and mixing from the double cover and metaplectic cover of the A_5 modular group," *Physical Review D*, vol. 103, no. 9, article 095013, 2021.

[47] M. G. Aartsen, R. Abbasi, Y. Abdou et al., "First observation of PeV-energy neutrinos with icecube," *Physical Review Letters*, vol. 111, article 021103, 2013.

[48] M. G. Aartsen, M. Ackermann, J. Adams et al., "Observation of high-energy astrophysical neutrinos in three years of IceCube data," *Physical Review Letters*, vol. 113, article 101101, 2014.

[49] M. G. Aartsen, K. Abraham, M. Ackermann et al., "Evidence for astrophysical muon neutrinos from the Northern Sky with IceCube," *Physical Review Letters*, vol. 115, article 081102, 2015.

[50] The IceCube Collaboration, "Detection of a particle shower at the Glashow resonance with IceCube," *Nature*, vol. 591, pp. 220–224, 2021.

[51] S.-J. Rong and D.-H. Xu, "The nonsymmetric flavor transition matrix and the apparent P violation," *Advances in High Energy Physics*, vol. 2022, Article ID 6949022, 11 pages, 2022.

[52] D.-H. Xu and S.-J. Rong, "Matter effects on flavor transitions of high-energy astrophysical neutrinos based on different decoherence schemes," 2022, https://arxiv.org/abs/2205.03164.

[53] M. G. Aartsen, R. Abbasi, M. Ackermann et al., "IceCube-Gen2: the window to the extreme universe," *Journal of Physics G: Nuclear and Particle Physics*, vol. 48, article 060501, 2021.

[54] N. Song, S. W. Li, C. A. Argüelles, M. Bustamante, and A. C. Vincent, "The future of high-energy astrophysical neutrino flavor measurements," *Journal of Cosmology and Astroparticle Physics*, vol. 4, p. 54, 2021.

[55] D.-H. Xu and S.-J. Rong, "The geometric correlations of leptonic mixing parameters," https://arxiv.org/abs/2207.05371.